EXPERIMENTAL MODELING OF INDUCTIVE DISCHARGES

Gaétan Chevalier and Francis F. Chen
Electrical Engineering Department
and
Institute of Plasma and Fusion Research

PPG – 1464 October 1992

This paper is to be presented at the American Vacuum Society, Chicago, IL, Nov. 1992.
To be published in *J. Vac. Sci. Technol. A.*

MS #930

EXPERIMENTAL MODELING OF INDUCTIVE DISCHARGES

G. Chevalier and F.F. Chen, UCLA

The density profile and efficiency of inductively excited helicon wave discharges are found to be sensitive to parameters not usually considered in theoretical treatments. A diverging magnetic field in the antenna region increases the central density by a factor of five and the total plasma production by a factor of two. A carbon or boron nitride aperture limiter also increases the density, but only if placed under a particular part of the antenna. Theoretical modeling can be carried out only after the important variables are found by exploratory measurements such as these.

EXPERIMENTAL MODELING OF INDUCTIVE DISCHARGES

Gaétan Chevalier and Francis F. Chen
Electrical Engineering Department
University of California, Los Angeles 90024-1495

I. INTRODUCTION

Capacitive rf plasma discharges are widely used in the semiconductor industry for etching and deposition processes. Computer modeling is commonly used to understand and improve the performance of such devices[1,2]. Recently, inductively coupled devices employing magnetic fields have been used for the same purpose. Resonant excitation methods are in general more efficient than the non-resonant ones[3]. Inductive discharges have more variable parameters than capacitives ones, and it is not yet clear which parameters are important enough to warrant extensive numerical analysis.

In a theoretical analysis of the helicon wave discharge, Chen[4-6] suggested that the high rate of energy absorption may be due to Landau damping of the helicon wave. Subsequent experiments by the authors and other groups have verified this hypothesis. On the other hand, the theoretical model of a uniform plasma in a uniform magnetic field does not necessarily represent the experimental situation. In this paper we give evidence that effects not usually considered in theoretical studies have a significant influence on the helicon discharge. More detailed theory, including computational modeling, can be done usefully only after a stage of *experimental modeling*, in which the important experimental parameters are found.

II. THEORETICAL BACKGROUND

Since the theory has been extensively published elsewhere[4-6], we will outline here only the main features needed for the understanding of the results presented.

Helicon waves are bounded whistler waves in the frequency range well below the electron gyro-frequency but well above the lower hybrid frequency. Thus, in a first approximation the electron

gyro-motion can be neglected together with all ion motions. In a bounded cylinder, the waves are not purely electromagnetic but have an important electrostatic component. For either an insulated or a conducting cylinder filled with uniform plasma of density n_o in a uniform magnetic field B_o, waves of the form exp[i(mθ+kz-ωt)] follow the dispersion relation[6]

$$\frac{n_o}{B_o} = \frac{\alpha}{\mu_o e} \frac{k_{\|}}{\omega} \tag{1}$$

where $k_{\|}$ is the component of the total wave number k parallel to the magnetic field, and α is given by the boundary condition

$$m\alpha J_m(k_\perp a) + kaJ_m'(k_\perp a) = 0, \tag{2}$$

where $\alpha^2 = k_\perp^2 + k_{\|}^2$ and $J_m'(k_\perp a)$ is the r-derivative of the Bessel function $J_m(k_\perp r)$ evaluated at r=a. For $k_{\|} << k_\perp$, Eq. (2) is approximately $J1(k_\perp a) = 0$, or $k_\perp \cong 3.83/a$ for the lowest radial mode.

III. EXPERIMENTS

Fig. 1 shows a schematic diagram of the apparatus. The quartz vacuum chamber has inside radius a= 2, 4, and 5 cm depending on the experiment, and is 0.9 to 1.7 m long. Results with the 2-cm tube have been published previously[5]. Here we give new results with the 4- and 5-cm tubes. For the 4 cm tube, two probes were used, the first probe was placed 25 cm, and the second, 50 cm from the antenna's midplane. For the 5-cm-diameter tube the configuration was similar, except that the upstream probe was closer to the antenna (13 cm from the midplane of the antenna).

The 12 magnetic field coils have the relative dimensions shown; the mounting flanges leave 1.23 cm gaps between the coils for diagnostics. The resulting field is uniform to ±5% and can be raised to 1.3 kG. To avoid water cooling and damage to the probe,

both the field and the rf are pulsed for ≤ 0.1 sec with about 5% duty cycle. The two coils at each end are connected to a separate power supply so that the field shape can be controlled. A description of the antennas used can be found in Ref. 6.

A. 4-cm-DIAMETER TUBE

Some of our experiments with the 4-cm-diameter tube have also been published in Ref. 6. We found in that paper that a 4-cm-diameter tube housing a 2-cm-diameter plasma acts as a reservoir of gas which can feed radially into the plasma to supply the flux of neutrals necessary to produce densities of order 10^{14} cm^{-3}. For that reason, we fed argon at four ports distributed along the machine and also increased the diameter to 5 cm, the largest that could fit within the magnetic coil structure. We report here new results that have not been published yet except in conference proceedings[8]. At the densities we obtained in this set of experiments the sputtering of tungsten probe tips would change the collection area during a run. This was remedied by using carbon tips (0.3 mm pencil lead) 1.5 mm long, centered in an alumina tube of 1.6 mm o.d.

The effect of varying the magnetic field shape is shown in Fig. 2, which gives the density on axis vs. voltage on the end coils for two antennas: a right-hand helical and a plane-polarized Nagoya Type III. The standard conditions were B = 600 G, p = 3 mTorr of argon, and P_{rf} = 1.9 kW at 27.12 MHz. A voltage of +40 gives a nearly uniform field and a voltage of -40 gives a strongly cusped field. The density from a plane-polarized antenna increases about a factor of 5 with a cusp field. The density increase is smaller with the right-hand helical antenna, because this gives a peaked profile even in a uniform field. Fig. 3 shows the density profiles with a uniform field, with the end coils off, and with the end coils reversed. Part of the density increase is due to the peaking of the profile with cusped fields, but the integrated density is also increased by a factor of 2.

We next investigated the effect of material limiters, carbon disks with holes of 1.2 and 2.0 cm. The density profiles with the 1.2-cm limiter are shown in Fig. 4(a) for a uniform B-field, and in Fig. 4(b) for a cusped B-field (end coils reversed). Other conditions were the same as above. Fig. 4(a) shows that the density was sensitive to the position of the limiter: a large increase in density occurred when

the limiter was located just under the rear loop of the antenna at -6 cm from the midplane of the antenna. When a cusped field was added (Fig. 4(b)), the profile was more sharply peaked, and the density further increased, showing that a magnetic limiter is more effective. In this case, the position of the limiter was not important, except when located well downstream, near the probe (+22 cm). Restricting the column at that point decreased the density.

Fig. 5(a) shows a comparison between a magnetic limiter and a material limiter for the optimum position (-6 cm). It can be shown that the cusp B-field is more efficient in confining the discharge than a carbon limiter. The combined effect of magnetic and material limiters is shown in Fig. 5(b), which shows the density on axis under standard conditions for different positions of the 1.2-cm limiter as the end coil voltage is varied. Since the limiter is effective at the rear end of the antenna (-6 cm), there is relatively little improvement with a cusp field. When the limiter is at the front end of the antenna, however, there is a great improvement with a cusped field, since the performance in a uniform field is so poor. These observations are not yet understood.

Even a solid carbon block affects the density, depending on its position. Fig. 6 shows the density profiles with the block at the rear end of the antenna (-6 cm), far back near the pump (-22 cm), and in between (-12 cm). There is an increase in density at the -6 cm position. Possible explanations include image currents in the limiter, reflection of helicon waves by the limiter, and the recirculation of neutral atoms formed by recombination of ions on the surface. Finally, Fig. 7 shows the performance of a limiter with a 2-cm-diameter hole. These data were taken for a uniform B-field. The effect of constricting the discharge diameter is much weaker than with the 1.2-cm hole.

To obtain the highest density with the available rf power, we operated at 1 kG with a cusped field, with no limiter, using a helical antenna along with a probe located near it. The importance of gas feed is shown in the pressure scan of Fig. 8(a). The density pulse had a peak of about 5 msec, followed by a plateau for the remainder of the 100-msec pulse. The peak density did not vary with pressure above a few mTorr, but the plateau density fell off at low pressures, indicating a deficiency in neutral gas. Apparently, unless the flow rate is very high, densities of the order of 10^{14} cm^{-3} are sustained only by the gas stored inside the tube, feeding radially into the

plasma. Fig. 8(b) shows radial profiles at the peak and the plateau for the upstream probe, as well as for the downstream probe, which does not show a density spike at the beginning of the pulse. The field was increased to 1.2 kG. There was a large axial density gradient because of the high pressure of 20-30 mTorr. At normal operating pressure, the plasma is much more uniform along the axis.

B. 5-cm-DIAMETER TUBE

To maximize the volume of the gas plenum, we increased the tube diameter to the largest that would fit within the coils. For the experiments with this tube diameter we used carbon tips identical to those used with the 4-cm-diameter tube. The standard conditions reported for the 4-cm tubes were also used here unless otherwise specified.

The density profiles for uniform B-fields (+45 V end coil voltage) and for cusped B-fields (0 V) are shown for the upstream and downstream probes in Figs. 9(a) and (b), respectively. The profile of Fig. 9(a) is not complete because of the restriction on the inward motion of the probe due to the type of port we used in order to be closer to the antenna. It can be observed from these figures that the downstream density does not change much with the cusp field (0 V) but is greatly reduced in a uniform B-field. The profile with the cusp field also became narrower. This shows the good confinement obtained with the cusp field and the efficiency of the helicon mode down 50 cm from the antenna midplane for normal pressure (p = 3 mTorr).

Fig. 9(c) and (d) shows the same thing but at high pressure (p= 60 mTorr) and with reversed end coil current (-30 V) . It can be seen from Fig. 9(c) that reversing the B-field does not increase the density notably compared with the 0 V case. In Fig. 9(d) the density downstream has decreased about one order of magnitude, showing the effect of collisional damping.

Next we investigate the effect of a solid carbon block on the discharge. The carbon block was placed between the antenna and the pumping unit at three locations: -6, -12, and -22 cm from the midplane of the antenna. These data were taken for a uniform B-field at a pressure of 3 mTorr. Fig. 10(a) shows that the highest density was obtained when the solid carbon block was exactly under

the back ring of the antenna. This result is similar to the one obtained with the 4-cm-diameter tube (see Fig. 7). In Fig. 10(b) are shown the downstream density profiles for the same conditions. One can see that the density at -6 cm has became about a quarter of its upstream value while the change for -22 cm is less than a factor of two. This has not been explained yet.

Next we made measurements with a carbon limiter with a 1.2-cm hole. This limiter was placed successively at these locations: -22, -12, -6, 0, +6, +12, and +22 cm from the midplane of the antenna. Figs. 11(a) and (c) show the profiles with the upstream probe with uniform B-field and with cusped B-field (0 end coil current), respectively. Figs. 11(b) and (d) show the same but for the downstream probe. We can see from Figs. 11(a) and (c) that the effect of the B-field is very small, showing that the carbon limiter is very effective here even at the front end of the antenna. It is worthwhile to mention here that the lowest density is obtained when the carbon limiter is directly under the midplane of the antenna, and the density increases slowly when going away from it towards the probes. At the center position, a complete change of tuning for the rf power was necessary. This is indicative of a large change in the resistance of the antenna. For the downstream results, it can be seen from Figs. 11(b) and (d) that when the limiter is behind the antenna (-6, -12, -22 cm), the density for both uniform and cusped B-fields is still about one third of the upstream density. The density for the limiter in front of the antenna is much lower, becoming higher when the limiter is moved away from the antenna. It seems that the closer the carbon limiter is to the center of the antenna, the more it affects the density and the antenna coupling.

To test if the fact that the carbon limiter is a conductor has an effect, we decided to do the same set of measurements with an insulating boron nitride limiter. Due to a fabrication error, the hole in this limiter had a diameter of 1.8 cm. The results are shown in Figs. 12 (a) to (d). From Figs. 12(a) and (c), the upstream measurements show that the density increases slightly with the presence of the cusped B-field for all positions of the limiter. The same happens downstream (Figs. 12(b) and (d)). Since this effect was not seen for the 1.2-cm carbon limiter it would be interesting to see if the effect of the cusped B-field would be visible for a 1.2 cm boron nitride limiter. It can be also observed from Figs. 12(a) and (c) that the position of the boron nitride limiter is much less critical when it is behind the antenna than for a carbon limiter, but it can

also be observed that the density is very low at all locations in front of the antenna. These results show a behavior for the boron nitride limiter that is different from the carbon limiter. The data for the boron nitride limiter placed directly under the antenna are missing because of the appearance of relaxation oscillations at that position, and a meaningful density measurement could not be obtained. Because of the differing hole diameters, the differences between the conducting and insulating limiters is not entirely clear. What is clear is that even an insulating limiter has the effect of increasing the axial density.

IV. SUMMARY

Data taken with the 4-cm-diameter tube show the effectiveness of cusped B-fields and carbon limiters in increasing the density of a helicon discharge. The data taken with the 5-cm-diameter tube show that the nature of the limiter placed inside the discharge makes a difference, and that a non-conducting limiter is also effective in confining the discharge if it is placed behind the antenna (not in the region where high density is needed). This paper has also shown the importance of magnetic field shaping near the antenna and of arranging for radial gas feed. None of the effects reported here were anticipated in the original theory. Our current ideas on what may be happening involve the interaction of nonlinear currents with the axial and radial components of the dc magnetic field, and the stabilizing effect of favorable magnetic curvature.

Since there is no need for internal electrodes in this device, it should be possible to produce arbitrarily long plasma columns of density 10^{14} cm^{-3} by adding antennas periodically. Other investigators[9,10] have found that, above a power threshold of 2-3 kW, the helicon discharge can burn out all the neutral atoms near the axis and constrict itself to a narrow, fully ionized column. We hope to add enough power to see this in the near future.

ACKNOWLEDGMENTS

This work was supported by the National Science Foundation, Grant No. ECS-8901249, and by the University of Wisconsin Engineering Research Center for Plasma Aided Manufacturing. We are grateful to M. Light for collaboration on the experiment.

REFERENCES

[1]M.A. Lieberman, J. Appl. Phys. **65**, 4186 (1989).

[2]G.R. Misium, A.J. Lichtenberg, and M.A. Lieberman, J. Vac. Sci. Technol. **A7**, 1007 (1989).

[3]G. Lisitano, R.A. Ellis Jr., W.M. Hooke, and T.H. Stix, Rev. Sci. Instrum. **39**, 295 (1968).

[4]F.F. Chen, in Proceedings of the Second International Conference on Plasma Physics, Kiev, 1987, ed. by A.G. Sitenko (Naukova Dumka, Kiev, 1977), Vol. 4, p. 321.

[5]F.F. Chen, Laser Part. Beams **7**, 551 (1989).

[6]F.F. Chen and G. Chevalier, J. Vac. Sci. Technol. **A10**, 1389 (1992).

[7]F.F. Chen and C.D. Decker, Plasma Phys. and Controlled Fusion **34**, 635 (1992).

[8]F.F. Chen and G. Chevalier, Proceedings of the Int'l Conf. of Plasma Physics, Innsbruck, Austria, 1701 (1992).

[9]P. Zhu and R.W. Boswell, Phys. Fluids **B3**, 869 (1991).

[10]A. Komori, T. Shoji, K. Miyamoto, J. Kawai, and Y. Kawai, Phys. Fluids **B3**, 893 (1991).

FIGURE CAPTIONS

Fig. 1. Schematic of the apparatus.

Fig. 2. Density on axis vs. voltage on the end coils. In the figures n_{13} stands for density in units of 10^{13} cm^{-3}.

Fig. 3. Density profiles with a uniform field, with the end coils off (cusp field), and with the end coils reversed (strong cusp field). The numbers refer to the relative densities integrated over the cross sections.

Fig.4. Density profiles with the 1.2-cm carbon limiter for a) uniform B-field and b) cusped B-field (end coils reversed).

Fig. 5. (a) Comparison of density profiles with magnetic and material limiters. The numbers give the r-weighted integral as in Fig. 3. (b) Combined effect of magnetic limiter and the 1.2-cm carbon limiter vs. end coil voltage. The density is taken on axis under standard conditions, -23, -12, -6, +6, and +22 cm from the center of the antenna.

Fig. 6. Density profiles with the solid carbon limiter, -6, -12, and -22 cm from the midplane of the antenna.

Fig. 7. Density profiles with the 2-cm carbon limiter at 0, -6, and +12 cm from the midplane of the antenna.

Fig. 8. (a) Density vs. pressure scan for the beginning of the rf power pulse (peak) and for the remainder of the pulse (plateau). (b) Radial density profiles at the peak and plateau for the upstream and downstream probes.

Fig. 9. Density profiles with no end coil current (0 V) and with a positive current (+45 V, uniform B-field) for (a) the upstream probe and (b)the downstream probe for normal pressure (p= 3 mTorr); and for strongly cusped B-field (-30 V), cusped B-field (0 V), and uniform B-field (+45 V) for (c) the upstream probe and (d) the downstream probe for high pressure (p= 60 mTorr).

Fig.10.Density profiles for a carbon block placed -6, -12, and -22 cm from the midplane of the antenna (a) for the upstream probe and (b) for the downstream probe.

Fig.11. Density profiles for a 1.2-cm carbon limiter placed -22, -12, -6, 0, +6, +12 and +22 cm from the midplane of the antenna for (a) a uniform B-field and (c) a cusped B-field for the upstream probe, and for (b) a uniform B-field and (d) a cusped B-field for the downstream probe.

Fig.12. Density profiles for a 1.8-cm boron nitride limiter placed -22, -12, -6, 0, +6, +12 and +22 cm from the midplane of the antenna for (a) a uniform B-field and (c) a cusped B-field for the upstream probe, and for (b) a uniform B-field and (d) a cusped B-field for the downstream probe.

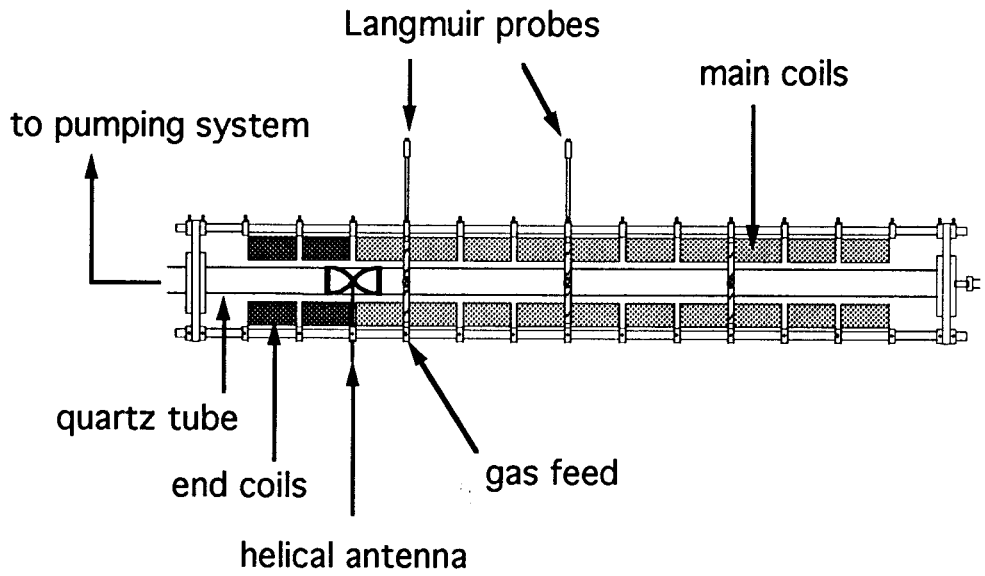
Langmuir probes
main coils
to pumping system
quartz tube
end coils
gas feed
helical antenna

Fig. 1

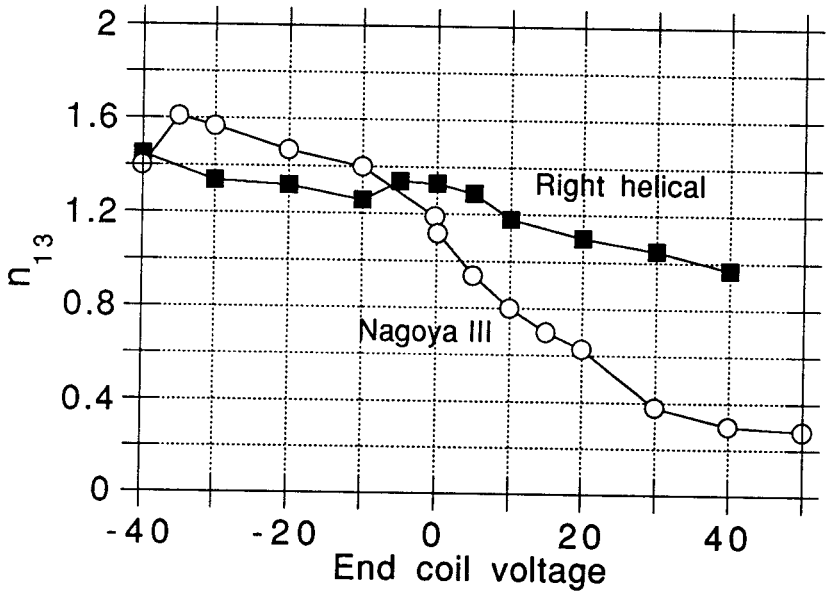
2
1.6
1.2
0.8
0.4
0
n_{13}
Right helical
Nagoya III
-40
-20
0
20
40
End coil voltage

Fig. 2

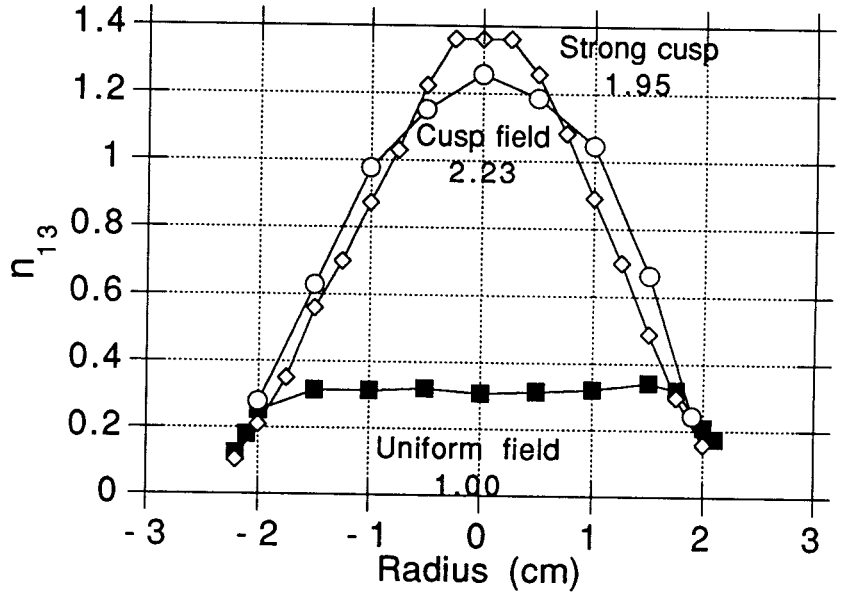
1.4
1.2
1
0.8
0.6
0.4
0.2
0
n_{13}
Strong cusp
1.95
Cusp field
2.23
Uniform field
1.00
-3
-2
-1
0
1
2
3
Radius (cm)

Fig. 3

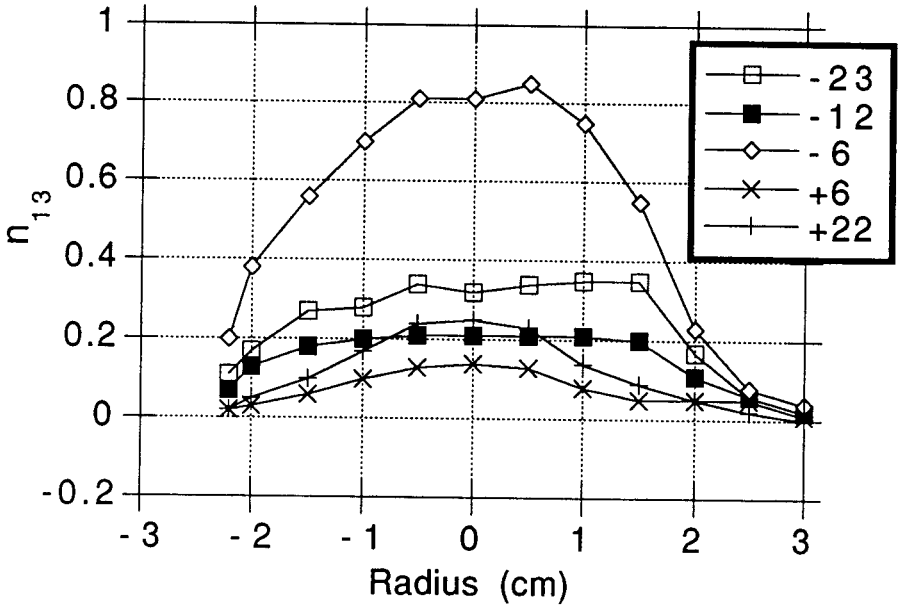

Fig. 4 (A)

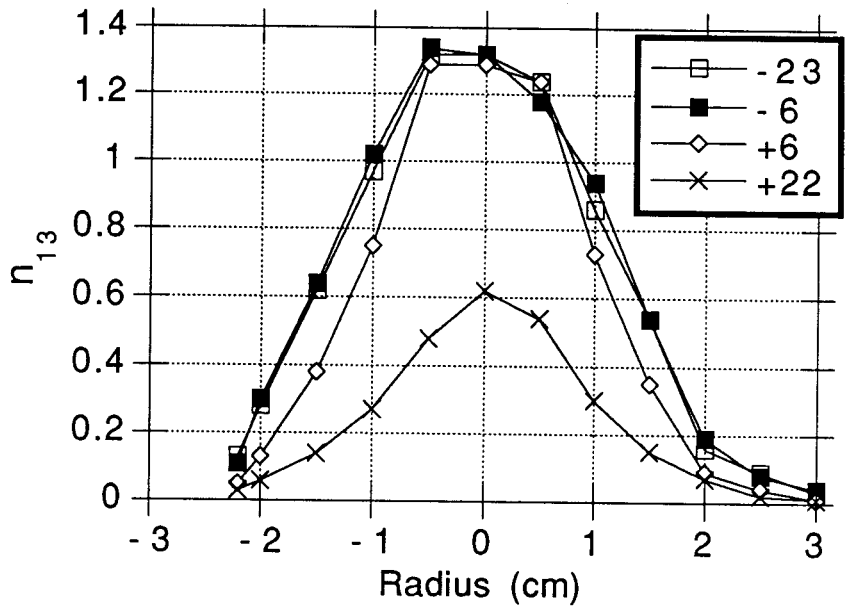

Fig. 4 (B)

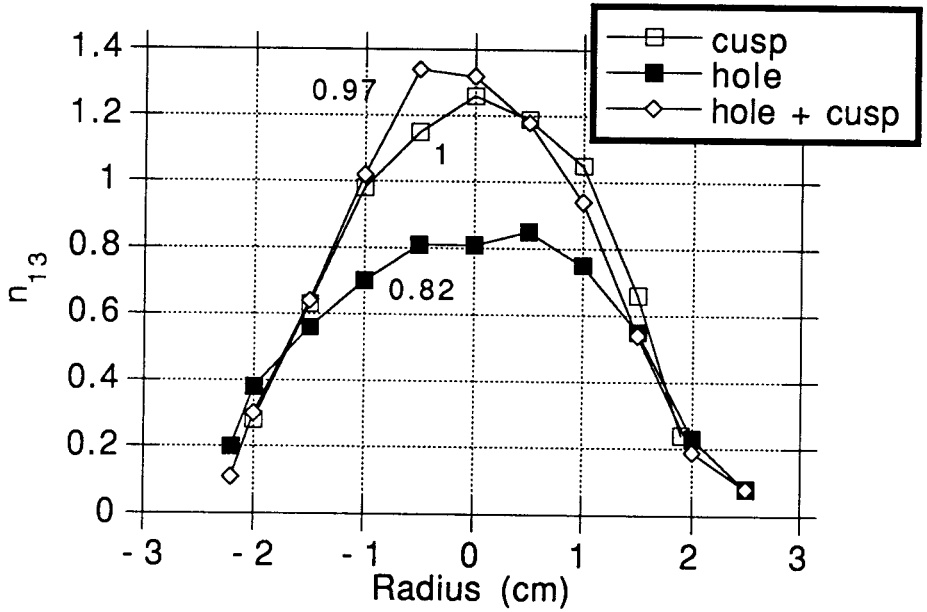

Fig. 5 (A)

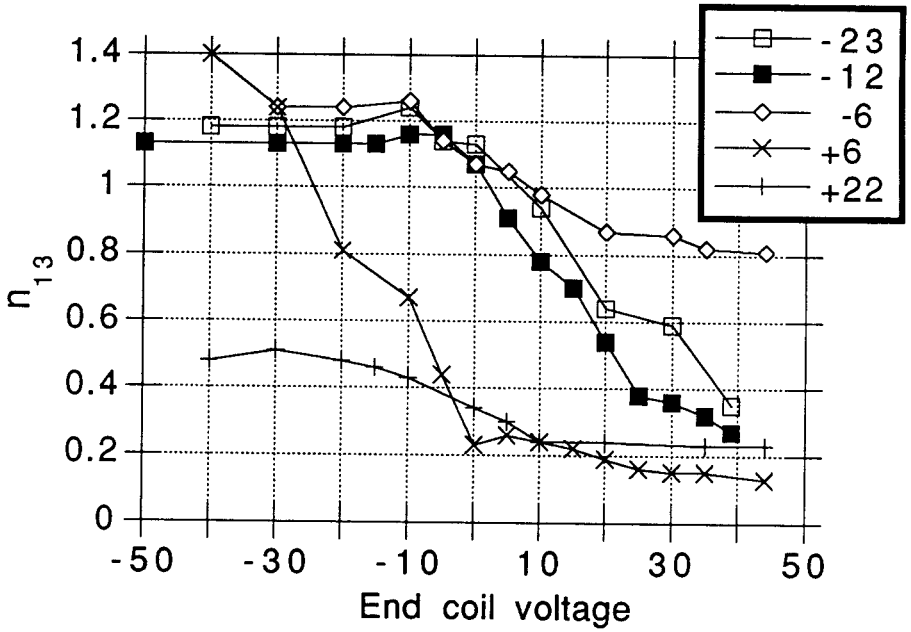

Fig. 5 (B)

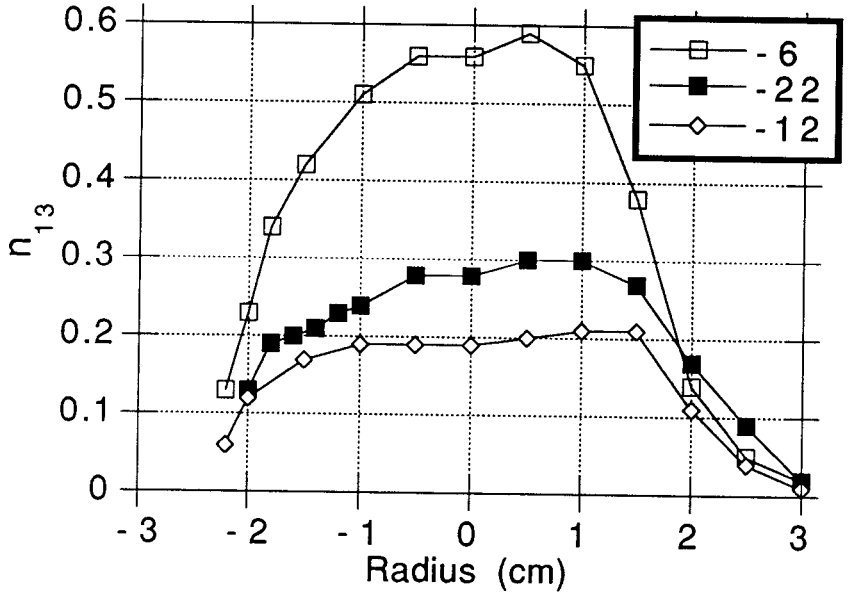
0.6
0.5
0.4
0.3
0.2
0.1
0
n_{13}
- 3
- 2
- 1
0
1
2
3
Radius (cm)
- 6
- 22
- 12

Fig. 6

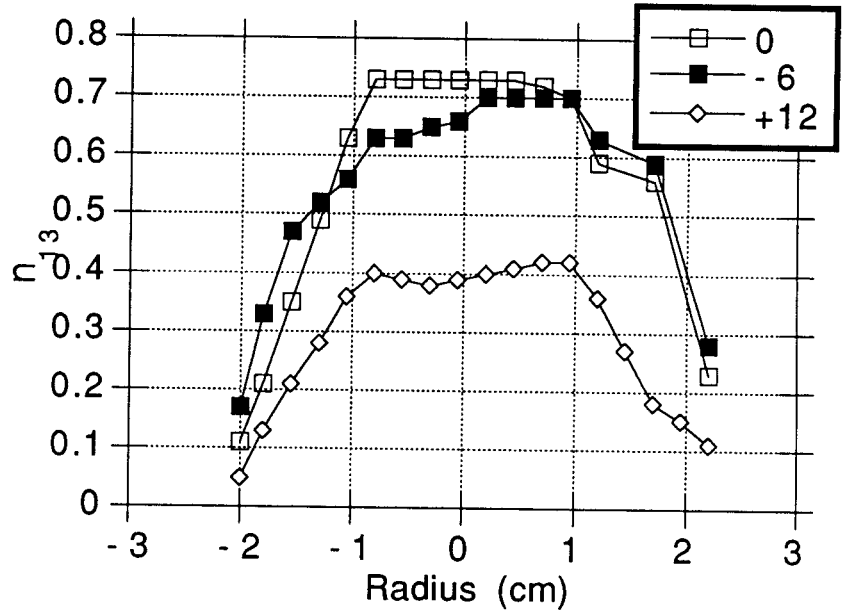
0.8
0.7
0.6
0.5
0.4
0.3
0.2
0.1
0
n_{13}
- 3
- 2
- 1
0
1
2
3
Radius (cm)
0
- 6
+12

Fig. 7

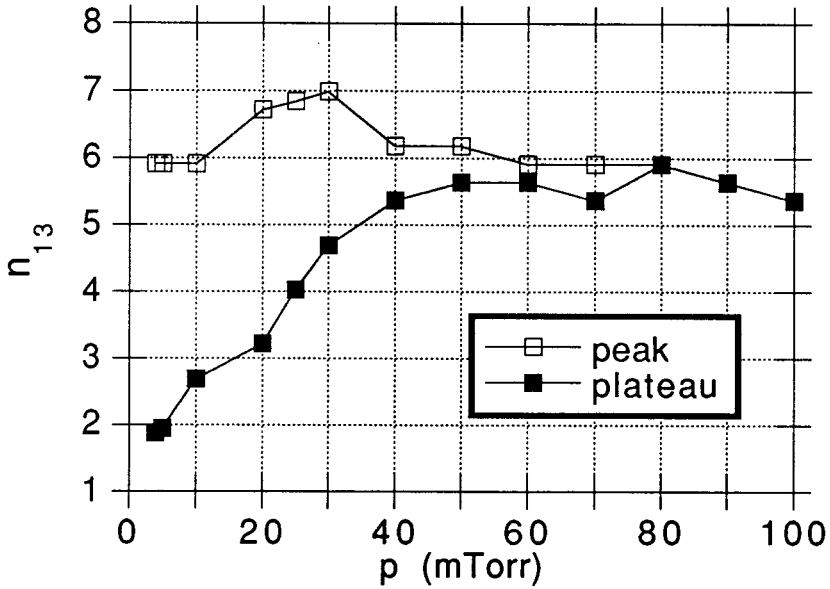
8
7
6
5
4
3
2
1
n_{13}
0
20
40
60
80
100
p (mTorr)
peak
plateau

Fig. 8 (A)

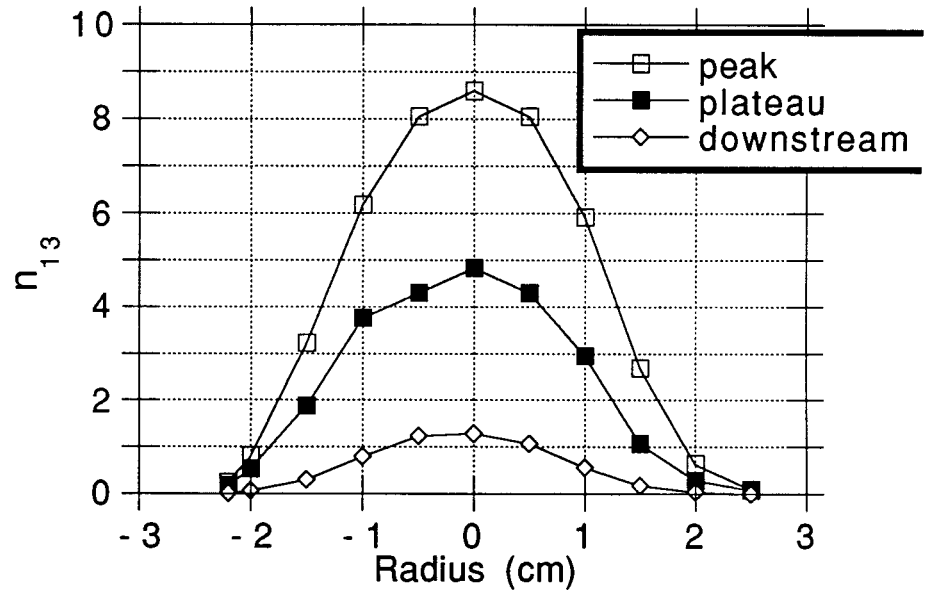
10
8
6
4
2
0
n_{13}
- 3
- 2
- 1
0
1
2
3
Radius (cm)
peak
plateau
downstream

Fig. 8 (B)

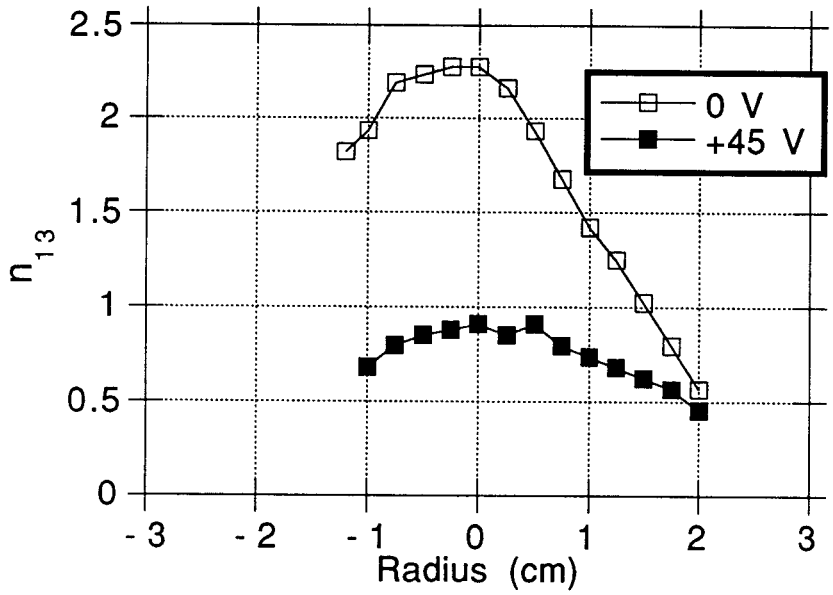

Fig. 9 (A)

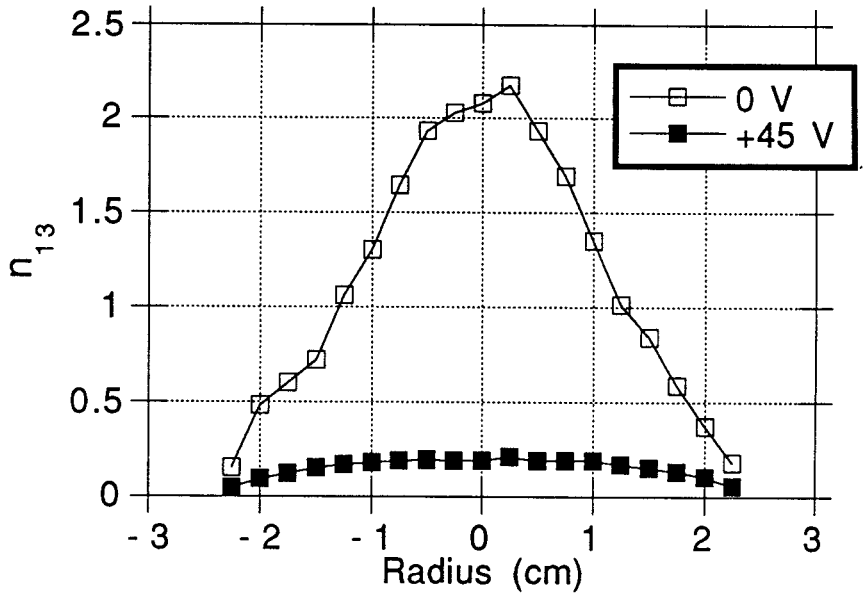

Fig. 9 (B)

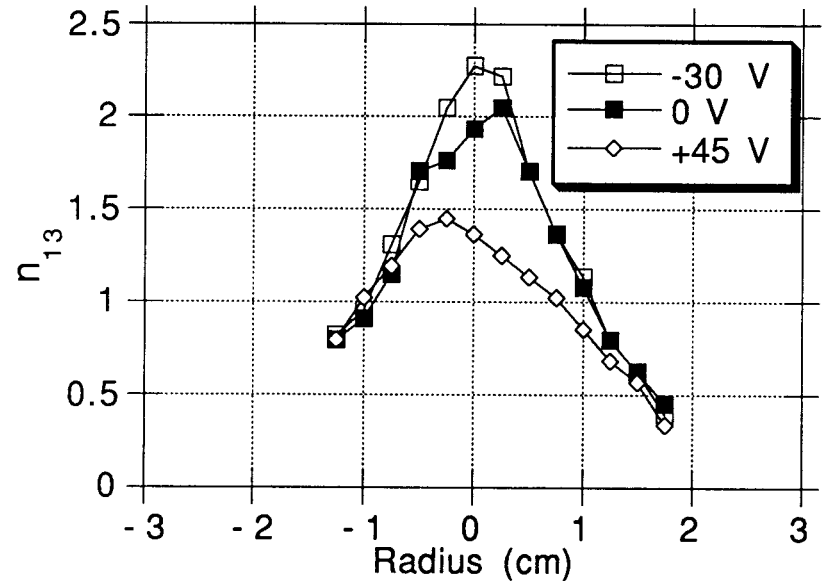

Fig. 9 (C)

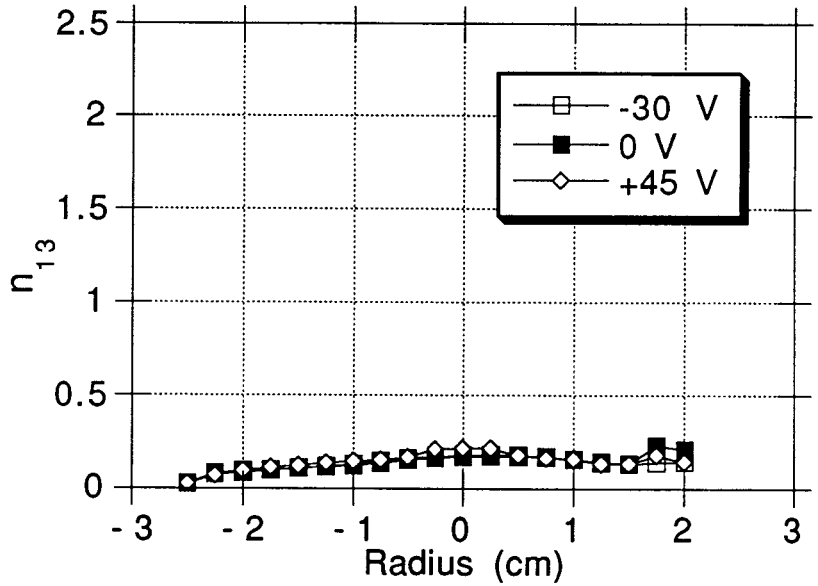

Fig. 9 (D)

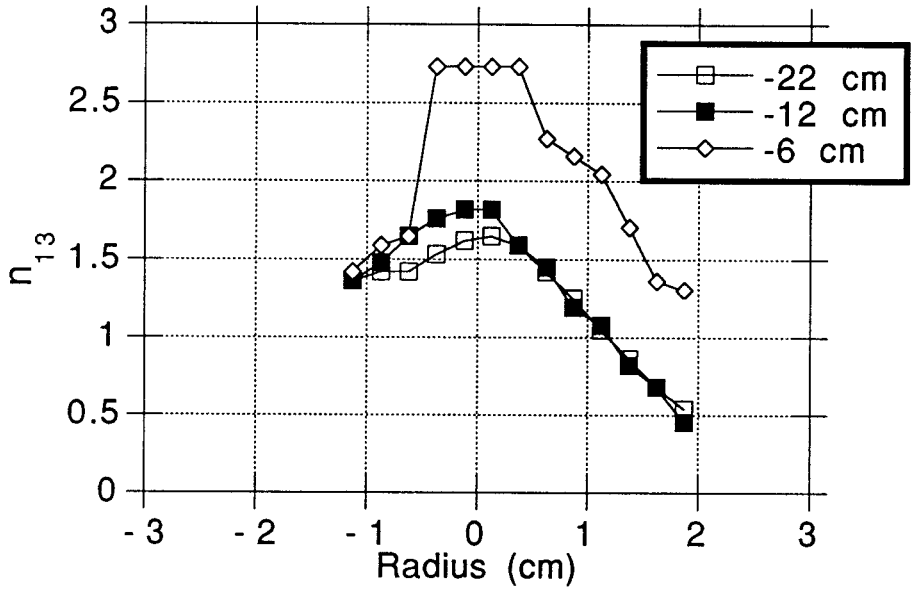

Fig. 10 (A)

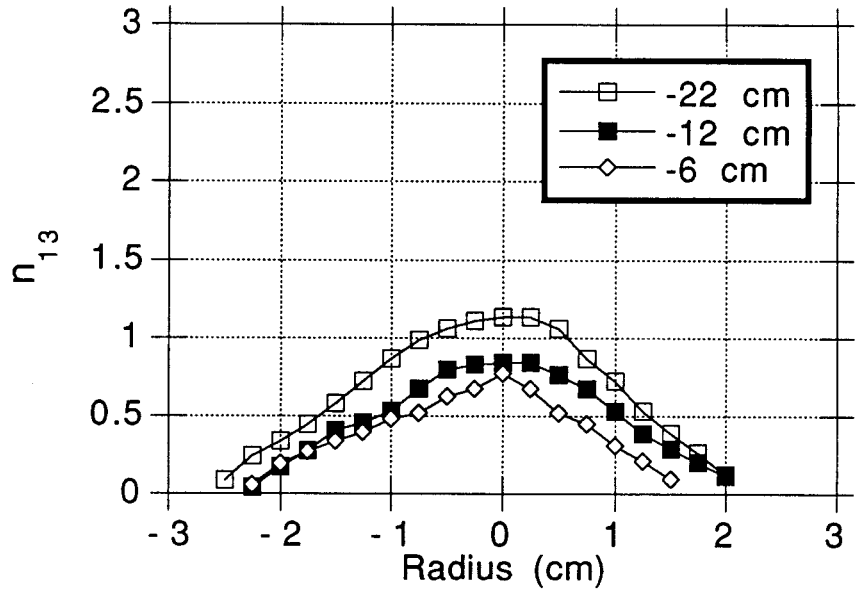

Fig. 10 (B)

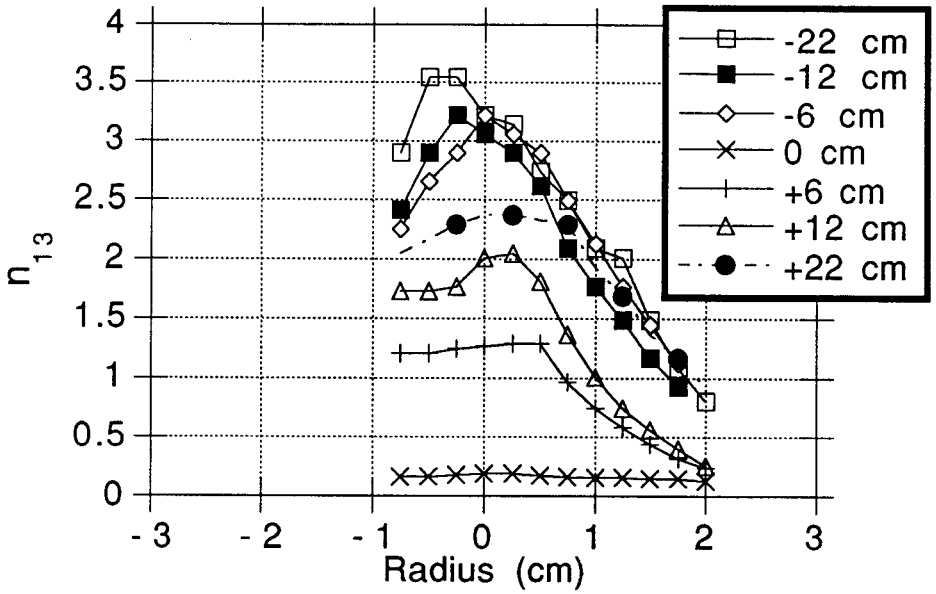

Fig. 11 (A)

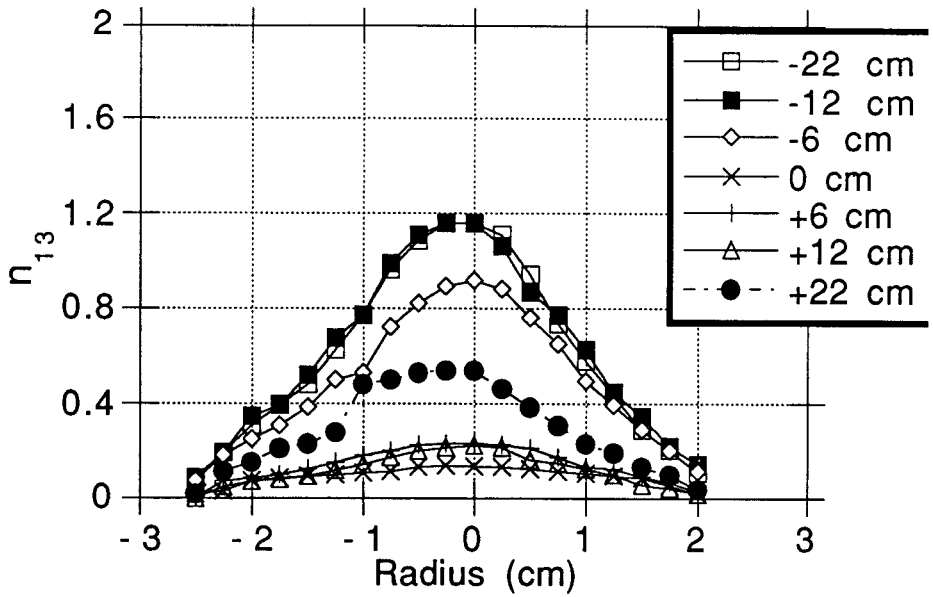

Fig. 11 (B)

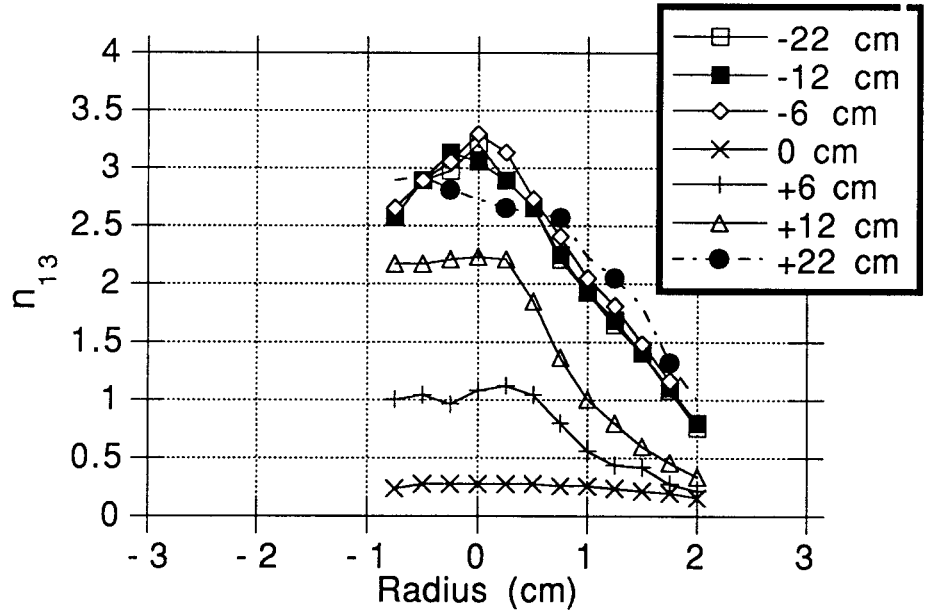

Fig. 11 (C)

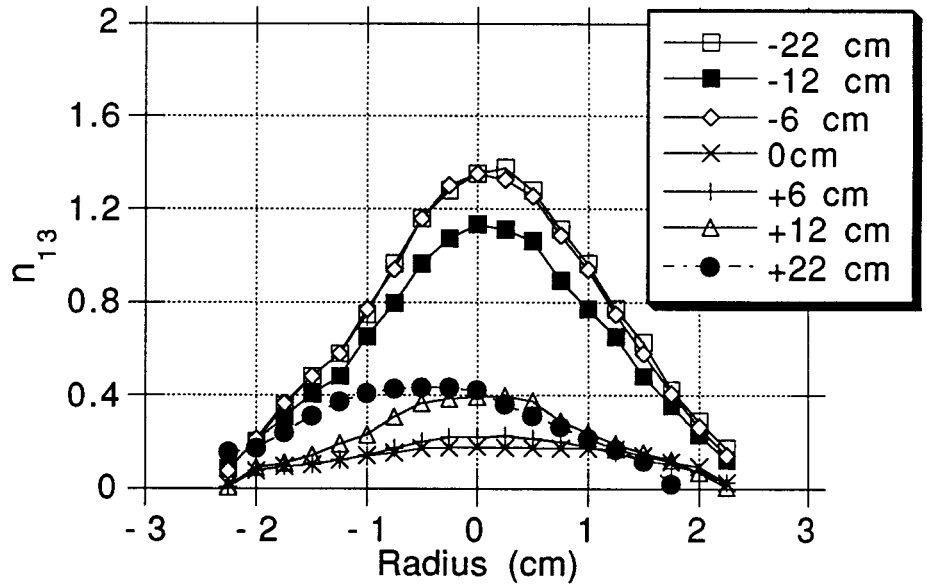

Fig. 11 (D)

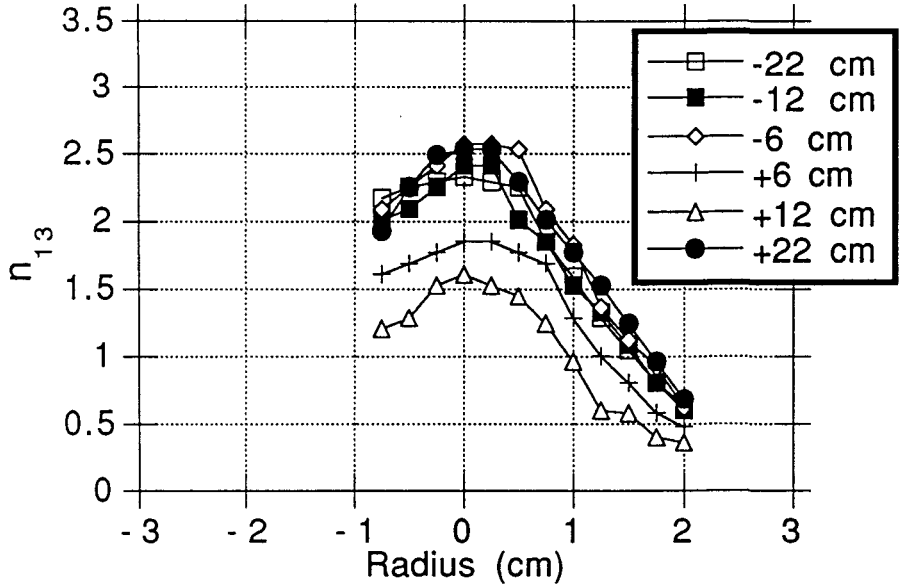

Fig. 12 (A)

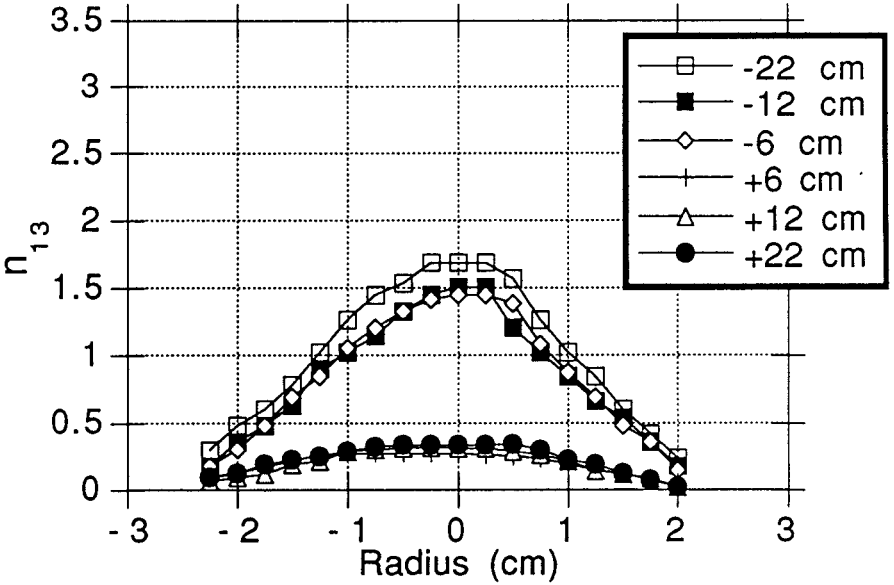

Fig. 12 (B)

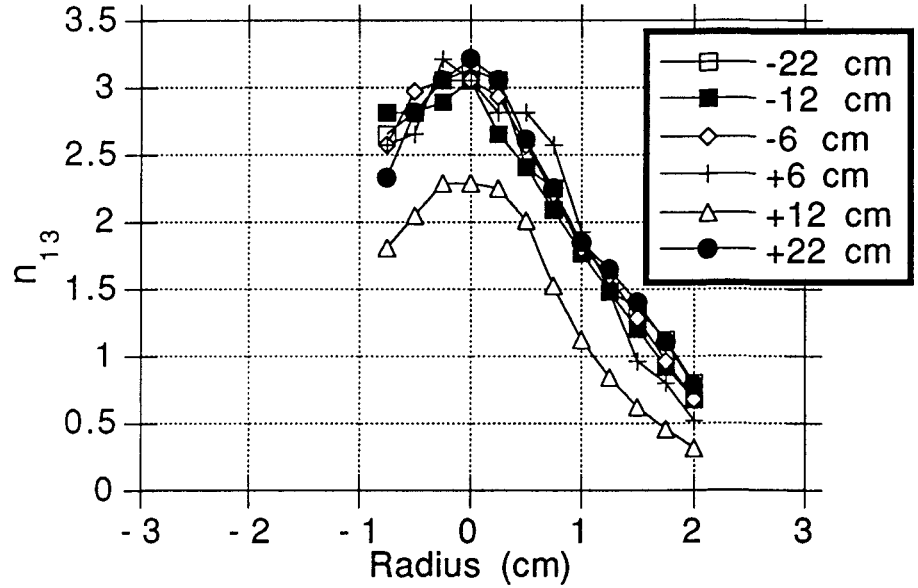

Fig. 12 (C)

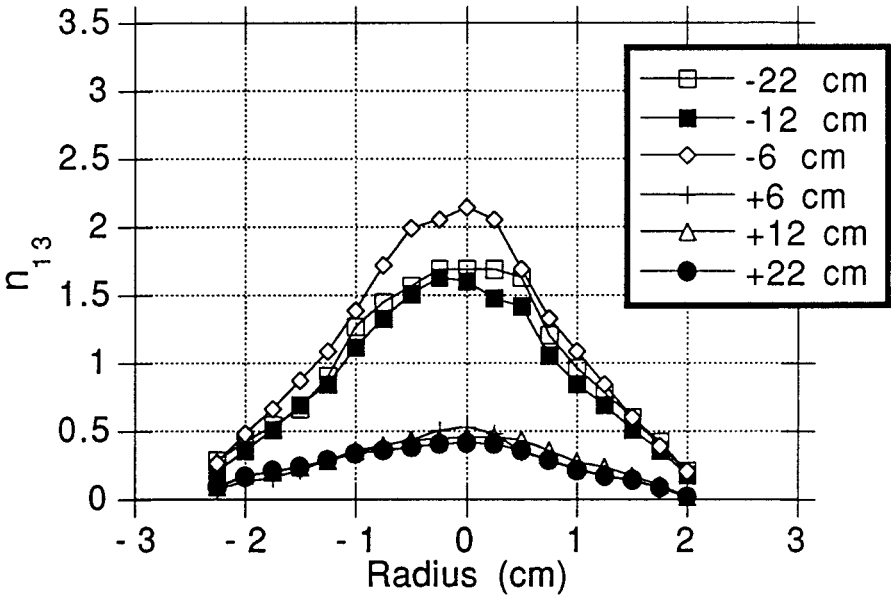

Fig. 12 (D)